Isolated electrons and muons in events with missing transverse momentum at HERA

V. Andreev, B. Andrieu, T. Anthonis, A. Astvatsatourov, A. Babaev, J. Bahr, P. Baranov, E. Barrelet, W. Bartel, S. Baumgartner, et al.

DESY 02-224
January 2003
ISSN 0418-9833

Isolated electrons and muons in events with missing transverse momentum at HERA

H1 Collaboration

Abstract

A search for events with a high energy isolated electron or muon and missing transverse momentum has been performed at the electron–proton collider HERA using an integrated luminosity of 13.6 pb^{-1} in e^-p scattering and 104.7 pb^{-1} in e^+p scattering. Within the Standard Model such events are expected to be mainly due to W boson production with subsequent leptonic decay. In e^-p interactions one event is observed in the electron channel and none in the muon channel, consistent with the expectation of the Standard Model. In the e^+p data a total of 18 events are seen in the electron and muon channels compared to an expectation of 12.4 ± 1.7 dominated by W production (9.4 ± 1.6). Whilst the overall observed number of events is broadly in agreement with the number predicted by the Standard Model, there is an excess of events with transverse momentum of the hadronic system greater than 25 GeV with 10 events found compared to 2.9 ± 0.5 expected. The results are used to determine the cross section for events with an isolated electron or muon and missing transverse momentum.

To be submitted to *Phys. Lett.* **B**

V. Andreev[24], B. Andrieu[27], T. Anthonis[4], A. Astvatsatourov[35], A. Babaev[23], J. Bähr[35], P. Baranov[24], E. Barrelet[28], W. Bartel[10], S. Baumgartner[36], J. Becker[37], M. Beckingham[21], A. Beglarian[34], O. Behnke[13], A. Belousov[24], Ch. Berger[1], T. Berndt[14], J.C. Bizot[26], J. Böhme[10], V. Boudry[27], J. Bracinik[25], W. Braunschweig[1], V. Brisson[26], H.-B. Bröker[2], D.P. Brown[10], D. Bruncko[16], F.W. Büsser[11], A. Bunyatyan[12,34], A. Burrage[18], G. Buschhorn[25], L. Bystritskaya[23], A.J. Campbell[10], S. Caron[1], F. Cassol-Brunner[22], V. Chekelian[25], D. Clarke[5], C. Collard[4], J.G. Contreras[7,41], Y.R. Coppens[3], J.A. Coughlan[5], M.-C. Cousinou[22], B.E. Cox[21], G. Cozzika[9], J. Cvach[29], J.B. Dainton[18], W.D. Dau[15], K. Daum[33,39], M. Davidsson[20], B. Delcourt[26], N. Delerue[22], R. Demirchyan[34], A. De Roeck[10,43], E.A. De Wolf[4], C. Diaconu[22], J. Dingfelder[13], P. Dixon[19], V. Dodonov[12], J.D. Dowell[3], A. Dubak[25], C. Duprel[2], G. Eckerlin[10], D. Eckstein[35], V. Efremenko[23], S. Egli[32], R. Eichler[32], F. Eisele[13], M. Ellerbrock[13], E. Elsen[10], M. Erdmann[10,40,e], W. Erdmann[36], P.J.W. Faulkner[3], L. Favart[4], A. Fedotov[23], R. Felst[10], J. Ferencei[10], S. Ferron[27], M. Fleischer[10], P. Fleischmann[10], Y.H. Fleming[3], G. Flucke[10], G. Flügge[2], A. Fomenko[24], I. Foresti[37], J. Formánek[30], G. Franke[10], G. Frising[1], E. Gabathuler[18], K. Gabathuler[32], J. Garvey[3], J. Gassner[32], J. Gayler[10], R. Gerhards[10], C. Gerlich[13], S. Ghazaryan[4,34], L. Goerlich[6], N. Gogitidze[24], S. Gorbounov[35], C. Grab[36], V. Grabski[34], H. Grässler[2], T. Greenshaw[18], G. Grindhammer[25], D. Haidt[10], L. Hajduk[6], J. Haller[13], B. Heinemann[18], G. Heinzelmann[11], R.C.W. Henderson[17], H. Henschel[35], O. Henshaw[3], R. Heremans[4], G. Herrera[7,44], I. Herynek[29], M. Hildebrandt[37], M. Hilgers[36], K.H. Hiller[35], J. Hladký[29], P. Höting[2], D. Hoffmann[22], R. Horisberger[32], A. Hovhannisyan[34], M. Ibbotson[21], Ç. İşsever[7], M. Jacquet[26], M. Jaffre[26], L. Janauschek[25], X. Janssen[4], V. Jemanov[11], L. Jönsson[20], C. Johnson[3], D.P. Johnson[4], M.A.S. Jones[18], H. Jung[20,10], D. Kant[19], M. Kapichine[8], M. Karlsson[20], O. Karschnick[11], J. Katzy[10], F. Keil[14], N. Keller[37], J. Kennedy[18], I.R. Kenyon[3], C. Kiesling[25], P. Kjellberg[20], M. Klein[35], C. Kleinwort[10], T. Kluge[1], G. Knies[10], B. Koblitz[25], S.D. Kolya[21], V. Korbel[10], P. Kostka[35], R. Koutouev[12], A. Koutov[8], J. Kroseberg[37], K. Krüger[10], J. Kueckens[10], T. Kuhr[11], M.P.J. Landon[19], W. Lange[35], T. Laštovička[35,30], P. Laycock[18], A. Lebedev[24], B. Leißner[1], R. Lemrani[10], V. Lendermann[10], S. Levonian[10], B. List[36], E. Lobodzinska[10,6], B. Lobodzinski[6,10], N. Loktionova[24], V. Lubimov[23], S. Lüders[37], D. Lüke[7,10], L. Lytkin[12], N. Malden[21], E. Malinovski[24], S. Mangano[36], P. Marage[4], J. Marks[13], R. Marshall[21], H.-U. Martyn[1], J. Martyniak[6], S.J. Maxfield[18], D. Meer[36], A. Mehta[18], K. Meier[14], A.B. Meyer[11], H. Meyer[33], J. Meyer[10], S. Michine[24], S. Mikocki[6], D. Milstead[18], S. Mohrdieck[11], M.N. Mondragon[7], F. Moreau[27], A. Morozov[8], J.V. Morris[5], K. Müller[37], P. Murín[16,42], V. Nagovizin[23], B. Naroska[11], J. Naumann[7], Th. Naumann[35], P.R. Newman[3], F. Niebergall[11], C. Niebuhr[10], G. Nowak[6], M. Nozicka[30], B. Olivier[10], J.E. Olsson[10], D. Ozerov[23], V. Panassik[8], C. Pascaud[26], G.D. Patel[18], M. Peez[22], E. Perez[9], A. Petrukhin[35], J.P. Phillips[18], D. Pitzl[10], R. Pöschl[26], I. Potachnikova[12], B. Povh[12], J. Rauschenberger[11], P. Reimer[29], B. Reisert[25], C. Risler[25], E. Rizvi[3], P. Robmann[37], R. Roosen[4], A. Rostovtsev[23], S. Rusakov[24], K. Rybicki[6], D.P.C. Sankey[5], E. Sauvan[22], S. Schätzel[13], J. Scheins[10], F.-P. Schilling[10], P. Schleper[10], D. Schmidt[33], D. Schmidt[10], S. Schmidt[25], S. Schmitt[37], M. Schneider[22], L. Schoeffel[9], A. Schöning[36], T. Schörner-Sadenius[25], V. Schröder[10], H.-C. Schultz-Coulon[7], C. Schwanenberger[10], K. Sedlák[29], F. Sefkow[37], I. Sheviakov[24], L.N. Shtarkov[24], Y. Sirois[27], T. Sloan[17], P. Smirnov[24], Y. Soloviev[24], D. South[21], V. Spaskov[8], A. Specka[27], H. Spitzer[11], R. Stamen[7], B. Stella[31], J. Stiewe[14], I. Strauch[10], U. Straumann[37], S. Tchetchelnitski[23], G. Thompson[19], P.D. Thompson[3], F. Tomasz[14], D. Traynor[19], P. Truöl[37], G. Tsipolitis[10,38], I. Tsurin[35], J. Turnau[6], J.E. Turney[19], E. Tzamariudaki[25], A. Uraev[23],

M. Urban[37], A. Usik[24], S. Valkár[30], A. Valkárová[30], C. Vallée[22], P. Van Mechelen[4], A. Vargas Trevino[7], S. Vassiliev[8], Y. Vazdik[24], C. Veelken[18], A. Vest[1], A. Vichnevski[8], V. Volchinski[34], K. Wacker[7], J. Wagner[10], R. Wallny[37], B. Waugh[21], G. Weber[11], R. Weber[36], D. Wegener[7], C. Werner[13], N. Werner[37], M. Wessels[1], B. Wessling[11], M. Winde[35], G.-G. Winter[10], Ch. Wissing[7], E.-E. Woehrling[3], E. Wünsch[10], A.C. Wyatt[21], J. Žáček[30], J. Zálešák[30], Z. Zhang[26], A. Zhokin[23], F. Zomer[26], and M. zur Nedden[25]

[1] *I. Physikalisches Institut der RWTH, Aachen, Germany*[a]
[2] *III. Physikalisches Institut der RWTH, Aachen, Germany*[a]
[3] *School of Physics and Space Research, University of Birmingham, Birmingham, UK*[b]
[4] *Inter-University Institute for High Energies ULB-VUB, Brussels; Universiteit Antwerpen (UIA), Antwerpen; Belgium*[c]
[5] *Rutherford Appleton Laboratory, Chilton, Didcot, UK*[b]
[6] *Institute for Nuclear Physics, Cracow, Poland*[d]
[7] *Institut für Physik, Universität Dortmund, Dortmund, Germany*[a]
[8] *Joint Institute for Nuclear Research, Dubna, Russia*
[9] *CEA, DSM/DAPNIA, CE-Saclay, Gif-sur-Yvette, France*
[10] *DESY, Hamburg, Germany*
[11] *Institut für Experimentalphysik, Universität Hamburg, Hamburg, Germany*[a]
[12] *Max-Planck-Institut für Kernphysik, Heidelberg, Germany*
[13] *Physikalisches Institut, Universität Heidelberg, Heidelberg, Germany*[a]
[14] *Kirchhoff-Institut für Physik, Universität Heidelberg, Heidelberg, Germany*[a]
[15] *Institut für experimentelle und Angewandte Physik, Universität Kiel, Kiel, Germany*
[16] *Institute of Experimental Physics, Slovak Academy of Sciences, Košice, Slovak Republic*[e,f]
[17] *School of Physics and Chemistry, University of Lancaster, Lancaster, UK*[b]
[18] *Department of Physics, University of Liverpool, Liverpool, UK*[b]
[19] *Queen Mary and Westfield College, London, UK*[b]
[20] *Physics Department, University of Lund, Lund, Sweden*[g]
[21] *Physics Department, University of Manchester, Manchester, UK*[b]
[22] *CPPM, CNRS/IN2P3 - Univ Mediterranee, Marseille - France*
[23] *Institute for Theoretical and Experimental Physics, Moscow, Russia*[l]
[24] *Lebedev Physical Institute, Moscow, Russia*[e]
[25] *Max-Planck-Institut für Physik, München, Germany*
[26] *LAL, Université de Paris-Sud, IN2P3-CNRS, Orsay, France*
[27] *LPNHE, Ecole Polytechnique, IN2P3-CNRS, Palaiseau, France*
[28] *LPNHE, Universités Paris VI and VII, IN2P3-CNRS, Paris, France*
[29] *Institute of Physics, Academy of Sciences of the Czech Republic, Praha, Czech Republic*[e,i]
[30] *Faculty of Mathematics and Physics, Charles University, Praha, Czech Republic*[e,i]
[31] *Dipartimento di Fisica Università di Roma Tre and INFN Roma 3, Roma, Italy*
[32] *Paul Scherrer Institut, Villigen, Switzerland*
[33] *Fachbereich Physik, Bergische Universität Gesamthochschule Wuppertal, Wuppertal, Germany*
[34] *Yerevan Physics Institute, Yerevan, Armenia*
[35] *DESY, Zeuthen, Germany*
[36] *Institut für Teilchenphysik, ETH, Zürich, Switzerland*[j]
[37] *Physik-Institut der Universität Zürich, Zürich, Switzerland*[j]

[38] *Also at Physics Department, National Technical University, Zografou Campus, GR-15773 Athens, Greece*
[39] *Also at Rechenzentrum, Bergische Universität Gesamthochschule Wuppertal, Germany*
[40] *Also at Institut für Experimentelle Kernphysik, Universität Karlsruhe, Karlsruhe, Germany*
[41] *Also at Dept. Fis. Ap. CINVESTAV, Mérida, Yucatán, México*[k]
[42] *Also at University of P.J. Šafárik, Košice, Slovak Republic*
[43] *Also at CERN, Geneva, Switzerland*
[44] *Also at Dept. Fis. CINVESTAV, México City, México*[k]

[a] *Supported by the Bundesministerium für Bildung und Forschung, FRG, under contract numbers 05 H1 1GUA /1, 05 H1 1PAA /1, 05 H1 1PAB /9, 05 H1 1PEA /6, 05 H1 1VHA /7 and 05 H1 1VHB /5*
[b] *Supported by the UK Particle Physics and Astronomy Research Council, and formerly by the UK Science and Engineering Research Council*
[c] *Supported by FNRS-FWO-Vlaanderen, IISN-IIKW and IWT*
[d] *Partially Supported by the Polish State Committee for Scientific Research, grant no. 2P0310318 and SPUB/DESY/P03/DZ-1/99 and by the German Bundesministerium für Bildung und Forschung*
[e] *Supported by the Deutsche Forschungsgemeinschaft*
[f] *Supported by VEGA SR grant no. 2/1169/2001*
[g] *Supported by the Swedish Natural Science Research Council*
[i] *Supported by the Ministry of Education of the Czech Republic under the projects INGO-LA116/2000 and LN00A006, by GAUK grant no 173/2000*
[j] *Supported by the Swiss National Science Foundation*
[k] *Supported by CONACyT*
[l] *Partially Supported by Russian Foundation for Basic Research, grant no. 00-15-96584*

1 Introduction

The HERA collaborations H1 and ZEUS have previously reported [1–3] the observation of events with an isolated high energy lepton and missing transverse momentum in e^+p collisions recorded during the period 1994–1997. The dominant Standard Model (SM) contribution to this topology is real W boson production with subsequent leptonic decay. Such events can also be a signature of new phenomena beyond the Standard Model [4]. H1 has reported [2] one e^- event and 5 $\mu^\pm$ events compared to expectations from the Standard Model of 2.4 ± 0.5 and 0.8 ± 0.2 for the $e^\pm$ and $\mu^\pm$ channels respectively, with W contributions of 1.65 ± 0.47 (e) and 0.53 ± 0.11 (μ). For the same data taking period ZEUS has reported [3] 3 (0) $e^\pm$ ($\mu^\pm$) events compared to an expectation of 2.1 (0.8) W events and 1.1 ± 0.3 (0.7 ± 0.2) events from other processes. In the present paper a search for events with isolated electrons[1] or muons and missing transverse momentum is performed in an extended phase space and with improved background rejection. The complete HERA I data sample (1994–2000) is analysed here. This corresponds to an integrated luminosity of 118.4 pb^{-1}, which represents a factor of three increase with respect to the previous published result.

This paper is organised as follows. Section 2 describes the SM processes that contribute to the signal and to the background. Section 3 describes the H1 detector and experimental conditions. Section 4 outlines the lepton identification criteria and the reconstruction methods for the hadronic final state. The selection requirements for the electron and muon channels are described in section 5. Studies of background processes are presented in section 6. Section 7 deals with systematic uncertainties and section 8 presents the results of the analysis including the numbers of events seen, the kinematics of the selected events and the measured cross sections. The results of a search for W production in the hadronic decay channel are given in section 9. The paper is briefly summarised in section 10.

2 Standard Model Processes

The processes within the Standard Model that are expected to lead to a final state containing an isolated electron or muon and missing transverse momentum, due to penetrating particles escaping detection in the apparatus, are described in detail in [2] and are only briefly outlined in this section. The processes are called "signal" if they produce events which contain a genuine isolated electron or muon and genuine missing transverse momentum in the final state. The processes are defined as "background" if they contribute to the selected sample through misidentification or mismeasurement. For the background processes, a fake lepton, fake missing transverse momentum or both can be reconstructed and may lead to the topology of interest. The following processes are considered.

***W* production**: $ep \to eW^\pm X$ or $ep \to \nu W^\pm X$ (signal)

Real W production in electron proton collisions with subsequent leptonic decay $W \to l\nu$, proceeding via photoproduction, is the dominant SM process that produces events with

[1] In this paper "electron" refers generically to both electrons and positrons. Where distinction is required the terms e^- and e^+ are used.

prominent high P_T isolated leptons and missing transverse momentum. W bosons are predicted to be produced mainly in resolved photon interactions, in which the W typically has small transverse momentum, whilst in direct photon interactions the W transverse momentum may be larger.

In this paper, the SM prediction for W production via $ep \rightarrow eW^{\pm}X$ is calculated by using a next to leading order (NLO) Quantum Chromodynamics (QCD) calculation [5] in the framework of the EPVEC [6] event generator. Each event generated by EPVEC according to its default LO cross section is weighted by a factor dependent on the transverse momentum and rapidity of the W [7], such that the resulting cross section corresponds to the NLO calculation. The ACFGP [8] parameterisation is used for the photon structure and the CTEQ4M [9] parton distribution functions are used for the proton. The renormalisation scale is taken to be equal to the factorisation scale and is fixed to the W mass. Final state parton showers are simulated using the PYTHIA framework [10].

The NLO corrections are found to be of the order of 30% at low W transverse momentum (resolved photon interactions) and typically 10% at high W transverse momentum (direct photon interactions) [5]. The NLO calculation reduces the theory error to 15% (from 30% at leading order).

The charged current process $ep \rightarrow \nu W^{\pm}X$ is calculated with EPVEC [6] and found to contribute less than 7% of the predicted signal cross section.

The total predicted W production cross section amounts to 1.1 pb for an electron–proton centre of mass energy of $\sqrt{s} = 300$ GeV and 1.3 pb for $\sqrt{s} = 318$ GeV.

Z production : $ep \rightarrow eZ(\rightarrow \nu\bar{\nu})X$ (signal)

A small number of signal events may be produced by Z production with subsequent decay to neutrinos. The outgoing electron from this reaction can scatter into the detector yielding the isolated lepton in the event while genuine missing transverse momentum is produced by the neutrinos. This process is calculated with the EPVEC generator and found to contribute less than 3% of the predicted signal cross section.

Charged Current (CC) processes : $ep \rightarrow \nu X$ (background)

A CC deep inelastic event can mimic the selected topology if a particle in the hadronic final state or a radiated photon is interpreted as an isolated lepton. The generator DJANGO [11] is used to calculate this contribution to the background.

Neutral Current (NC) processes : $ep \rightarrow eX$ (background)

The scattered electron in a NC deep inelastic event yields an isolated high energy lepton, but measured missing transverse momentum can only be produced by fluctuations in the detector response or by undetected particles due to limited geometrical acceptance. The generator RAPGAP [12] is used to calculate this contribution to the background.

Photoproduction of jets : $\gamma p \rightarrow X$ (background)

The generator PYTHIA [13] is used to calculate the contribution from hard scattering photoproduction processes. Background from this process may occur if a particle from

the hadronic final state is interpreted as an isolated lepton and missing transverse momentum is measured due to fluctuations in the detector response or limited geometrical acceptance.

Lepton pair (LP) production : $ep \to e\, l^+ l^- X$ (background)

Lepton pair production can mimic the selected topology if one lepton escapes detection and measurement errors cause apparent missing momentum. The generator GRAPE 1.1 [14], based on a full calculation of electroweak diagrams, is used. The dominant contribution is due to photon–photon processes and is cross-checked with the LPAIR [15] generator. Internal photon conversions are also calculated. Z production and its subsequent decay into charged leptons is also included in GRAPE. This contribution is found to be negligible.

In order to determine signal acceptances and background contributions, the detector response to events produced by the above programs is simulated in detail using a program based on GEANT [16]. The simulated events are then subjected to the same reconstruction and analysis chain as the data.

3 Experimental Conditions

Results are presented for the 37.0 pb^{-1} of e^+p data taken in 1994–1997 at an electron–proton centre of mass energy of $\sqrt{s} = 300$ GeV , the 13.6 pb^{-1} of e^-p data (1998–1999, $\sqrt{s} = 318$ GeV) and the 67.7 pb^{-1} of e^+p data (1999–2000, $\sqrt{s} = 318$ GeV).

A detailed description of the H1 detector can be found in [17]. Only those components of particular importance to this analysis are described here.

The inner tracking system consisting of central and forward[2] tracking detectors (drift chambers) is used to measure charged particle trajectories and to determine the interaction vertex. A solenoidal magnetic field allows the measurement of the particle transverse momenta.

Electromagnetic and hadronic final state particles are absorbed in a highly segmented Liquid Argon (LAr) calorimeter [18]. The calorimeter is 5 to 8 interaction lengths deep depending on the polar angle of the particle. A lead–fibre calorimeter (SpaCal) is used to detect backward going electrons and hadrons.

The LAr calorimeter is surrounded by a superconducting coil with an iron return yoke instrumented with streamer tubes. Tracks of muons, which penetrate beyond the calorimeter, are reconstructed from their hit pattern in the streamer tubes. The instrumented iron is also used as a backing calorimeter to measure the energy of hadrons that are not fully absorbed in the LAr calorimeter.

In the forward region of the detector a set of drift chamber layers (the forward muon system) detects muons and, together with an iron toroidal magnet, allows a momentum measurement. Around the beam pipe, the plug calorimeter measures hadronic activity at low polar angles.

[2]The forward direction and the positive z–axis are taken to be that of the proton beam direction. All polar angles are defined with respect to the positive z–axis.

The LAr calorimeter provides the main trigger for events with high transverse momentum. The trigger efficiency is $\simeq 98\%$ for events with an electron which has transverse momentum above 10 GeV. For events with high missing transverse momentum, determined from an imbalance in transverse momentum measured in the calorimeter $P_T^{\rm calo}$, the trigger efficiency is $\simeq 98\%$ when $P_T^{\rm calo} > 25$ GeV and is $\sim 50\%$ when $P_T^{\rm calo} = 12$ GeV [19]. Events may also be triggered by a pattern consistent with a minimum ionising particle in the muon system in coincidence with tracks in the tracking detectors.

4 Lepton Identification and Hadronic Reconstruction

An electron candidate is defined [20] by the presence of a compact and isolated electromagnetic cluster of energy in the LAr calorimeter, with the requirement of an associated track having an extrapolated distance of closest approach to the cluster of less than 12 cm. Electrons found in regions between calorimeter modules containing large amounts of inactive material are excluded [19]. The energy of the electron candidate is measured from the calorimeter cluster. The additional energy allowed within a cone of radius 1 in pseudorapidity–azimuth (η–ϕ) space around the electron candidate is required to be less than 3% of the energy attributed to the electron candidate. The efficiency of electron identification is established using NC events and is greater than 98% [19].

A muon candidate is identified by a track in the forward muon system or a charged track in the inner tracking system associated with a track segment or an energy deposit in the instrumented iron. The muon momentum is measured from the track curvature in the solenoidal or toroidal magnetic field. A muon candidate may have no more than 8 GeV deposited in the LAr calorimeter in a cone of radius 0.5 in (η–ϕ) space associated with its track. The efficiency to identify muons is established using elastic LP events [21] and is greater than 90%.

Identified leptons are characterised by the following variables, where l represents e or μ:

- P_T^l, the transverse momentum of an identified muon or electron;
- θ_l, the polar angle of the muon or electron.

In order to check that the probability to misidentify a particle as an electron or muon is well described by the simulation, a sample of NC events is used, in which a second electron or a muon is found in the event. In the majority of cases this second lepton results from the misidentification of a hadron from the final state. The second lepton in the event must pass the same criteria as described above, except for the upper limit on the calorimeter energy within a cone associated with its track. The study is performed requiring the reconstructed electrons or muons to have $P_T^l > 10$ GeV. From a total NC sample of 121408 events, 2087 events with a second identified electron and 520 events with a reconstructed muon are selected by this procedure. Figure 1a shows the polar angle distribution of the electron with the second highest transverse momentum and figure 1b shows the polar angle distribution of reconstructed muons. The distributions are described by the simulation within the uncertainties, demonstrating that the misidentification of a particle as an electron or muon is well understood.

The hadronic final state (HFS) is measured by combining calorimeter energy deposits with low momentum tracks as described in [19]. Identified isolated electrons or muons are excluded from the HFS. The calibration of the hadronic energy scale is made by comparing the transverse momentum of the precisely measured scattered electron to that of the HFS in a large NC event sample. The transverse momentum of the hadronic system is:

- P_T^X, which includes all reconstructed particles apart from identified isolated leptons.

The isolation of identified leptons with respect to jets or other tracks in the event is quantified using:

- their distance D_{jet} from the axis of the closest hadronic jet in η–ϕ space. For this purpose jets, excluding identified leptons, are reconstructed using an inclusive k_T algorithm [22–24] and are required to have transverse momentum greater than 5 GeV. If there is no such jet in the event, D_{jet} is defined with respect to the polar and azimuthal angles of the hadronic final state;
- their distance D_{track} from the closest track in η–ϕ space, where all tracks with a polar angle greater than 10° and transverse momentum greater than 0.15 GeV are considered.

The following quantities are sensitive to the presence of high energy undetected particles and/or can be used to reduce the main background contributions.

- $P_T^{\rm calo}$, the net transverse momentum measured from all energy deposits recorded in the calorimeter.
- $P_T^{\rm miss}$, the total missing transverse momentum reconstructed from all observed particles (electrons, muons and hadrons). $P_T^{\rm miss}$ differs most from $P_T^{\rm calo}$ in the case of events with muons, since they deposit little energy in the calorimeter.
- $\frac{V_{\rm ap}}{V_{\rm p}}$, a measure of the azimuthal balance of the event. It is defined as the ratio of the anti–parallel to parallel components of the measured calorimetric transverse momentum, with respect to the direction of the calorimetric transverse momentum [19]. Events with one or more high p_T particles that do not deposit much energy in the calorimeter (μ, ν) generally have low values of $\frac{V_{\rm ap}}{V_{\rm p}}$.
- $\delta_{\rm miss} = 2E_e - \sum_i E_i(1-\cos\theta_i)$, where E_i and θ_i denote the energy and polar angle of each particle in the event detected in the main detector ($\theta_e < 176^\circ$) and E_e is the electron beam energy. For an event where only momentum in the proton direction is undetected $\delta_{\rm miss}$ is zero.
- $\Delta\phi_{l-X}$, the difference in azimuthal angle between the lepton and the direction of P_T^X. NC events typically have values of $\Delta\phi_{l-X}$ close to 180°.
- $\zeta_e^2 = 4E_e^{'}E_e\cos^2\theta_e/2$, where $E_e^{'}$ is the energy of the final state electron. For NC events, where the scattered electron is identified as the isolated high transverse momentum electron, ζ_e^2 is equal to the four momentum transfer squared Q^2. Since the NC cross section falls steeply with Q^2, these events generally have small values of ζ_e^2. Conversely, electrons from W decay generally have high values of ζ_e^2.

5 Selection Criteria

The published H1 observation [2] using 1994–1997 e^+p data was based on the selection of a sample of events with $P_T^{\rm calo} > 25$ GeV. This experimental cut mainly selected charged current events in a phase space where the trigger efficiency is high. In the selected events all isolated charged tracks with transverse momentum above 10 GeV were identified as electrons or muons.

In the present paper the $P_T^{\rm calo}$ cut has been lowered to 12 GeV, taking advantage of the improved understanding of trigger efficiencies with increased luminosity and more sophisticated background rejection. The analysis extends the phase space towards lower missing transverse momentum for the electron channel ($P_T^{\rm calo} \simeq P_T^{\rm miss}$) and towards lower P_T^X for the muon channel ($P_T^{\rm calo} \simeq P_T^X$). The lepton identification has also been improved and extended in the forward direction. The increased phase space and increased luminosity allow the comparison with the SM predictions to be made differentially and with improved precision. Further details of the analysis can be found in [25, 26].

The selection criteria for both channels are summarised in table 1. The dominant background in the electron channel is due to NC and CC events. To reduce the NC background, events with NC topology (azimuthally balanced, with the lepton and the hadronic system back-to-back in the transverse plane) are rejected. For low values of $P_T^{\rm calo}$, where the NC background is largest, a requirement on ζ_e^2 is imposed. A requirement that the lepton candidate be isolated from the hadronic final state is imposed to reject CC events. Events which have, in addition to an isolated electron, one or more isolated muons are not considered in the electron channel, but may contribute in the muon channel. The dominant backgrounds in the muon channel are inelastic muon pair production and CC or photoproduction events which contain a reconstructed muon. The final muon sample is selected by rejecting azimuthally balanced events and events where more than one muon is observed.

Following the selection criteria described above, the overall efficiency to select SM $W \to e\nu$ events is 41% and to select SM $W \to \mu\nu$ events is 14%. The main difference in efficiency between the two channels is due to the cut on $P_T^{\rm calo}$, which for muon events acts as a cut on P_T^X because the muon deposits little energy in the calorimeter. There is thus almost no efficiency in the muon channel for $P_T^X < 12$ GeV. For values of $P_T^X > 25$ GeV the efficiencies of the two channels are compatible at $\sim 40\%$.

6 Background Studies

To verify that the backgrounds (see section 2) that contribute to the two channels are well understood, alternative event samples, each enriched in one of the important background processes, are compared with simulations. For both channels these event samples have the same basic phase space definition (θ_l, P_T^l, $P_T^{\rm calo}$) as the main analysis. It should be noted that these selections do not explicitly reject signal events, which may be present in the enriched samples.

The two background enriched samples in the electron channel, defined within the phase space $5^\circ < \theta_e < 140^\circ$, $P_T^e > 10$ GeV and $P_T^{\rm calo} > 12$ GeV, are selected with the following additional requirements.

Variable	Electron	Muon
θ_l	$5^\circ < \theta_l < 140^\circ$	
P_T^l	> 10 GeV	
$P_T^{\rm calo}$	> 12 GeV	
$P_T^{\rm miss}$	> 12 GeV	
P_T^X	–	> 12 GeV
D_{jet}	> 1.0	
D_{track}	> 0.5 for $\theta_e \geq 45^\circ$	> 0.5
ζ_l^2	> 5000 GeV^2 for $P_T^{\rm calo} < 25$ GeV	–
$\frac{V_{ap}}{V_p}$	< 0.5 (< 0.15 for $P_T^e < 25$ GeV)	< 0.5 (< 0.15 for $P_T^{\rm calo} < 25$ GeV)
$\Delta\phi_{l-X}$	$< 160^\circ$	$< 170^\circ$
# isolated μ	0	1
$\delta_{\rm miss}$	> 5 GeV †	–

† *if only one e candidate is detected, which has the same charge as the beam lepton.*

Table 1: Selection requirements for the electron and muon channels.

NC enriched sample
A NC dominated electron sample is selected by requiring $D_{jet} > 1.0$. The events in this channel mainly contain genuine electron candidates, but with missing transverse momentum arising from mismeasurement.

CC enriched sample
A CC dominated sample is obtained by rejecting events with an isolated muon and applying cuts to suppress the NC component. These criteria are $\zeta_e^2 \geq 2500$ GeV^2, $\frac{V_{ap}}{V_p} \leq 0.15$, $\delta_{\rm miss} > 5$ GeV and $\Delta\phi_{e-X} < 160^\circ$. In this sample the missing transverse momentum is genuine, but an electron candidate is usually falsely identified.

The two samples designed to study the backgrounds in the muon channel, defined within the same phase space $5^\circ < \theta_\mu < 140^\circ$, $P_T^\mu > 10$ GeV and $P_T^{\rm calo} > 12$ GeV, are selected with the following additional requirements.

LP enriched sample
A sample of events predominantly from the two photon process is selected by requiring at least one isolated muon and $\frac{V_{ap}}{V_p} \leq 0.2$ to suppress photoproduction events.

CC enriched sample A sample dominated by CC events is selected by requiring $\frac{V_{ap}}{V_p} \leq 0.15$ and requiring at least one muon candidate that need not be isolated. This selection tests fake or real muons observed in events with genuine missing P_T.

The distributions of all quantities used in these selections are well described in both shape and normalisation by the SM expectation in regions where there is little contribution from W production. This gives us confidence that the backgrounds are described within the uncertainty.

Example distributions of the background enriched event samples for the e^+p data are shown in figure 2 for the electron channel and in figure 3 for the muon channel. Also included in the figures are the SM expectations from all processes together and the signal expectation alone. Agreement is also obtained between the data and the simulation in all distributions for the e^-p data sample.

7 Systematic Uncertainties

The systematic uncertainties on quantities which influence the SM expectation and the measured cross section (see section 8.1) are presented in this section and discussed in more detail in [19,26]. The uncertainties on the signal expectation and the acceptance used in the cross section calculation are determined by varying experimental quantities by $\pm$ 1 standard deviation and recalculating the cross section or expectation. The experimental uncertainties are listed below and the corresponding variation of the cross section is given in table 2.

- **Leptonic quantities**
  The uncertainties on the θ_l and the ϕ_l measurements are 3 mrad and 1 mrad respectively. The electron energy scale uncertainty is 3%. The muon energy scale uncertainty is 5%.

- **Hadronic quantities**
  The uncertainties on the θ and ϕ measurements of the hadronic final state are both 20 mrad. The hadronic energy scale uncertainty is 4%. The error on the measurement of $\frac{V_{\rm ap}}{V_{\rm p}}$ is ± 0.02.

- **Triggering / Identification**
  The electron finding efficiency has an uncertainty of 2%. The muon finding efficiency has an error of 5% in the central ($\theta_\mu > 12.5^\circ$) region and 15% in the forward ($\theta_\mu < 12.5^\circ$) region. The uncertainty on the track reconstruction efficiency is 3%. The uncertainty on the trigger efficiency for the muon channel varies from 16% at $P_T^X = 12$ GeV to 2% at $P_T^X > 40$ GeV.

- **Luminosity**
  The luminosity measurement has an uncertainty of 1.5%.

- **Model**
  A 10% uncertainty on the model dependence of the acceptance is estimated by comparing the results obtained with two further generators which produce W bosons with different kinematic distributions from those of EPVEC. The generators used are an implementation of W production within PYTHIA and ANOTOP, an "anomalous top production" generator, using the matrix elements of the complete process $e + q \rightarrow e + t \rightarrow e + b + W$ as obtained from the CompHEP program [27].

Contributions from background processes, modelled using RAPGAP, DJANGO and GRAPE, are attributed 30% systematic errors determined from the level of agreement observed between

the simulations and the control samples (see section 6). The uncertainties associated with lepton misidentification and the production of fake missing transverse momentum are included in these errors.

A theoretical uncertainty of 15% is quoted for the predicted contributions from signal processes (predominantly SM W production). This is due mainly to uncertainties in the parton distribution functions and the scales at which the calculation is performed [5].

Source of systematic uncertainty	Error on measured cross section	
	$P_T^X < 25$ GeV	$P_T^X > 25$ GeV
Leptonic quantities	$\pm 0.6\%$	$\pm 0.6\%$
Hadronic quantities	$\pm 3.3\%$	$\pm 8.3\%$
Triggering/Identification	$\pm 3.7\%$	$\pm 4.7\%$
Luminosity	$\pm 1.5\%$	$\pm 1.5\%$
Model Uncertainty	$\pm 10\%$	$\pm 10\%$

Table 2: Summary of experimental systematic errors on the measured cross section in two regions of P_T^X.

8 Results

For the $e^- p$ data sample one event is observed in the electron channel. The kinematics of the event are listed in table 3. No events are observed in the muon channel. This compares well to the SM expectations of 1.69 ± 0.22 events in the electron channel and 0.37 ± 0.06 in the muon channel.

In the $e^+ p$ data sample 10 candidate events are observed in the electron channel compared to 7.2 ± 1.2 expected from signal processes and 2.68 ± 0.49 from background sources. One candidate event in the electron channel is observed to contain an e^-. This event was first reported and discussed in [2]. Four of the other candidate events contain an e^+. The charges of the electrons in the remaining five events are unmeasured since the electrons are produced at low polar angles and they shower in material in the tracking detectors. In the muon channel 8 candidate events are observed compared to 2.23 ± 0.43 expected from signal processes and 0.33 ± 0.08 from background sources. Four of the muon events observed in the $e^+ p$ data sample are among those first reported and discussed in [2]. The event discussed in [1] is rejected from this analysis by the azimuthal difference ($\Delta\phi_{\mu-X}$) cut. Four of the events have a positively charged muon, three have a negative muon and in one event the charge is not determined.

Distributions of the selected events in lepton polar angle, azimuthal difference, transverse mass and P_T^X are shown in figure 4. The lepton–neutrino transverse mass is defined as

$$M_T = \sqrt{(P_T^{\rm miss} + P_T^l)^2 - (\vec{P}_T^{\rm miss} + \vec{P}_T^l)^2}, \qquad (1)$$

where $\vec{P}_T^{\rm miss}$ and $\vec{P}_T^{l}$ are the vectors of the missing transverse momentum and isolated lepton respectively. The figure shows the electron and muon channels combined. Also included is the expectation of the Standard Model. The events generally have low values of lepton polar angle and are consistent with a flat distribution in azimuthal difference $\Delta\phi_{l-X}$, in agreement with the expectation. The distribution of the events in M_T is compatible with the Jacobian peak expected from W production. The kinematics of the events with $P_T^X > 25$ GeV are detailed in table 3.

In three of the eighteen events a further electron is detected in the main detector ($\theta_e < 176^\circ$). Taking this to be the scattered electron and assuming that there is only one neutrino in the final state and there is no initial state QED radiation, the lepton–neutrino mass $M_{l\nu}$ can be reconstructed. All three events yield masses that are consistent with the W mass, having values of 86^{+7}_{-9}, 73^{+7}_{-7} and 79^{+12}_{-12} GeV. The observation of a second electron in these three events is compatible with the expectation from SM W production, where approximately 25% of events have a scattered electron in the acceptance range of the main detector.

Details of the event yields from the e^+p data sample as a function of the transverse momentum of the hadronic final state, P_T^X, are given in table 4 and 5 for the electron and muon channels respectively. The combined results for the electron and muon channels are given in table 6. At $P_T^X < 25$ GeV eight events are seen, in agreement with the expectation from the Standard Model. At $P_T^X > 25$ GeV ten events are seen, six of which have $P_T^X > 40$ GeV, where the signal expectation is very low. The probability for the SM expectation to fluctuate to the observed number of events or more is 0.10 for the full P_T^X range, 0.0015 for $P_T^X > 25$ GeV and 0.0012 for $P_T^X > 40$ GeV. The uncertainties on the SM predictions are taken into account in calculating these probabilities.

An excess is observed at $P_T^X > 25$ GeV in both sets of e^+p data. In the 1994–1997 data 4 events are observed compared to an expectation of 0.80 ± 0.14. In the 1999–2000 data 6 events are observed compared to an expectation of 2.12 ± 0.36.

The method published in [2] has been applied to the 1999–2000 data sample. Using this method an excess of events is also seen at $P_T^X > 25$ GeV in this new data sample: 5 events are observed for 2.34 ± 0.29 expected. These 5 events selected by the method of the previously published analysis are also found by the analysis presented in this paper.

8.1 Cross Section

The observed number of events in the e^+p data sample is corrected for acceptance and detector effects to obtain a cross section for all processes yielding genuine isolated electrons or muons and missing transverse momentum. This is defined for the kinematic region $5^\circ < \theta_l < 140^\circ$, $P_T^l > 10$ GeV, $P_T^{\rm miss} > 12$ GeV and $D_{jet} > 1.0$ at a centre of mass energy[3] of $\sqrt{s} = 312$ GeV. The definition of isolated electrons or muons includes those from leptonic tau decay. The generator EPVEC is used to calculate the detector acceptance A for this region of phase space. The acceptance accounts for trigger and detection efficiencies and migrations. The cross section is thus

$$\sigma = \frac{(\mathrm{N_{data}} - \mathrm{N_{bgd}})}{\mathcal{L}A}, \tag{2}$$

[3]Assuming a linear dependence of the cross section on the proton beam energy.

where $\mathrm{N_{data}}$ is the number of events observed, $\mathrm{N_{bgd}}$ is the number of events expected from processes treated here as background (see section 2) and $\mathcal{L}$ is the integrated luminosity of the data sample.

The cross section integrated over the full P_T^X range is

$$\sigma = 0.31 \pm 0.10 \pm 0.04 \text{ pb}, \tag{3}$$

where the first error is statistical and the second is systematic (calculated as described in section 7).

This result is compatible with the SM signal expectation of 0.237 ± 0.036 pb, dominated by the process $ep \rightarrow eWX$, calculated at NLO [5, 7]. The small signal components from $ep \rightarrow \nu WX$ and Z production are calculated with EPVEC [6] as explained in section 2. The cross section is presented in table 7 split into the regions $P_T^X < 25$ GeV and $P_T^X > 25$ GeV. Whilst the cross section in the low P_T^X region agrees within errors with the prediction, in the high P_T^X region it exceeds the expectation. Table 7 also includes two signal calculations in which all components are calculated at LO [5,6]. The calculation in [6] is the default calculation implemented in the event generator EPVEC. All the calculations agree within the uncertainties.

9 Search for W Production in the Hadronic Decay Channel

Since the dominant SM process that produces events with isolated charged leptons and missing transverse momentum is W production, it is interesting to search for W bosons decaying hadronically. The search for hadronic W decays is performed using events with two high transverse momentum jets in 117.3 pb^{-1} of e^+p and e^-p data from the period 1995–2000.

Events are selected with at least two hadronic jets, reconstructed using an inclusive k_T algorithm, with a transverse momentum P_T greater than 25 GeV for the leading jet and greater than 20 GeV for the second highest P_T jet. The minimum P_T of any further jet considered in the event is set to 5 GeV. The pseudorapidity η of each jet is restricted to the range $-0.5 < \eta < 2.5$. The dijet combination with invariant mass M_{jj} closest to the W mass is selected as the W candidate. The resolution of the reconstructed W mass is approximately 5 GeV. P_T^X is defined as the transverse momentum of the hadronic system after excluding the W candidate jets.

A cut on the missing transverse momentum $P_T^{\mathrm{miss}} < 20$ GeV is applied to reject CC events and non–ep scattering background. NC events where the electron is misidentified as a jet are rejected [28, 29]. The final selection is made with the cuts $M_{jj} > 70$ GeV and $|\cos\hat{\theta}| < 0.6$, where $\hat{\theta}$ is the decay angle in the W rest frame, with the W flight direction in the laboratory frame taken as the quantisation axis. This phase space is chosen to optimise the acceptance for W events and reduce other SM contributions. The overall selection efficiency for SM W production is 43% and is 29% for $P_T^X > 40$ GeV.

The main physics background to this search is the production of jets via hard partonic scattering, which is modelled by PYTHIA and RAPGAP for the photoproduction and deep inelastic regimes respectively. The predicted cross section is increased by a factor of 1.2 in order to match the observed number of events outside the signal region.

The systematic uncertainty on the background prediction includes parton distribution function uncertainties, the uncertainty on the jet energy scale and uncertainties due to the misidentification of an electron as a jet. In quadratic sum these give a total systematic error on the background prediction of 23% [28, 30]. The SM W production rate has a theoretical error of 15%, which is added in quadrature to the experimental uncertainties, resulting in an overall error of 21%.

The M_{jj} distribution (without the M_{jj} cut) and the P_T^X distribution (with all cuts) of the selected data are compared to the Standard Model in figure 5. The final data selected show overall agreement with the SM expectation up to the highest P_T^X values. At $P_T^X > 25$ GeV, 126 events are observed compared to 162 ± 36 expected with 5.3 ± 1.1 from W production. The expectation is dominated by QCD multi–jet production. For $P_T^X > 40$ GeV 27 events are observed in the data, compatible with the expectation of 30.9 ± 6.7, where the W contribution amounts to 1.9 ± 0.4 events. Although there is increasing sensitivity to W production with increasing P_T^X, it is at present not possible to conclude from the hadronic channel whether the observed excess of events with an isolated electron or muon with missing transverse momentum at high P_T^X is due to W production.

10 Summary

A search for events with isolated electrons or muons and missing transverse momentum has been performed in e^+p and e^-p data, using the complete HERA I (1994-2000) data sample. The selection has been optimised to increase the acceptance for W production events and it extends to lower values of hadronic transverse momentum P_T^X than in previous publications.

One electron event and no muon events are observed in the e^-p data, consistent with the expectations of 1.69 ± 0.22 and 0.37 ± 0.06 for the electron and muon channels respectively in this relatively low luminosity data sample. In the e^+p data sample 10 events are observed in the electron channel and 8 in the muon channel. These events are kinematically consistent with W production. The expected numbers of events from the Standard Model are 9.9 ± 1.3 and 2.55 ± 0.44 for the electron and muon channels respectively.

At low P_T^X, the number of observed events in both channels is consistent with the expectation. At $P_T^X > 25$ GeV, however, the 10 observed events exceed the SM prediction of 2.92 ± 0.49. An excess of events is observed in both the 1994–1997 and the 1999–2000 e^+p data samples. The observed events are used to make a measurement of the cross section for all processes producing isolated electrons or muons and missing transverse momentum in the kinematic region studied.

In a separate search for hadronic W decays, agreement with the SM expectation is found up to the highest P_T^X values. The high background in this channel, however, does not allow one to conclude whether the excess of isolated leptons with missing P_T at high P_T^X is due to W production.

Acknowledgements

We are grateful to the HERA machine group whose outstanding efforts have made this experiment possible. We thank the engineers and technicians for their work in constructing and maintaining the H1 detector, our funding agencies for financial support, the DESY technical staff for continual assistance and the DESY directorate for support and for the hospitality which they extend to the non–DESY members of the collaboration. The authors wish to thank K.P. Diener and M. Spira for many useful discussions and for providing the NLO calculation for W production.

References

[1] H1 Collaboration, T. Ahmed *et al.*, DESY preprint 94–248 (1994).

[2] C. Adloff *et al.* [H1 Collaboration], Eur. Phys. J. C **5** (1998) 575 [hep-ex/9806009].

[3] J. Breitweg *et al.* [ZEUS Collaboration], Phys. Lett. B **471** (2000) 411 [hep-ex/9907023].

[4] T. Kon, T. Kobayashi and S. Kitamura, Phys. Lett. B **376**, (1996) 227 [hep-ph/9601338];
H. Fritzsch and D. Holtmannspötter, Phys. Lett. B **457** (1999) 186 [hep-ph/9901411];
C. Diaconu *et al.*, J. Phys. G **25** (1999) 1412 [hep-ph/9901335];
W. Rodejohann and K. Zuber, Phys. Rev. D **62** (2000) 094017 [hep-ph/0005270];
C. Adloff *et al.* [H1 Collaboration], Eur. Phys. J. C **17** (2000) 567 [hep-ex/0007035];
A. Belyaev, [hep-ph/0007058];
T. Kon, T. Kobayashi, S. Kitamura and T. Iimura, Phys. Lett. B **494**, (2000) 280 [hep-ph/0007200].

[5] K. P. Diener, C. Schwanenberger and M. Spira, Eur. Phys. J. C **25** (2002) 405 [hep-ph/0203269];
P. Nason, R. Rückl and M. Spira, J. Phys. G **25**, (1999) 1434 [hep-ph/9902296];
M. Spira, [hep-ph/9905469].

[6] U. Baur, J. A. Vermaseren and D. Zeppenfeld, Nucl. Phys. B **375** (1992) 3.

[7] M. Spira and K. P. Diener, private communication.

[8] P. Aurenche *et al.*, Z. Phys. C **56** (1992) 589.

[9] H. L. Lai *et al.*, Phys. Rev. D **55** (1997) 1280 [hep-ph/9606399].

[10] C. Diaconu, in Proc. of the Workshop on Monte Carlo Generators for HERA Physics, ed. A. Doyle *et al.*, DESY-PROC-1999-02, p.631.

[11] G. A. Schuler and H. Spiesberger, in Proc. of the Workshop on Physics at HERA, ed. W. Buchmüller and G. Ingelmann, DESY (1992), Vol. 3, p.1419.

[12] H. Jung, Comput. Phys. Commun. **86** (1995) 147.

[13] T. Sjöstrand, Comput. Phys. Commun. **82** (1994) 74.

[14] T. Abe *et al.*, in Proc. of the Workshop on Monte Carlo Generators for HERA Physics, ed. A. Doyle *et al.*, DESY-PROC-1999-02, p.566;

T. Abe, Comput. Phys. Commun. **136** (2001) 126 [hep-ph/0012029].

[15] S. P. Baranov, O. Dünger, H. Shooshtari and J. A. Vermaseren, in Proc. of the Workshop on Physics at HERA, ed. W. Buchmüller and G. Ingelmann, DESY (1992), Vol. 3, p.1478;

J. A. Vermaseren, Nucl. Phys. B **229** (1983) 347.

[16] R. Brun *et al.*, "GEANT3 User's Guide", CERN-DD/EE/84-1.

[17] I. Abt *et al.* [H1 Collaboration], Nucl. Instrum. Meth. A **386** (1997) 310;

I. Abt *et al.* [H1 Collaboration], Nucl. Instrum. Meth. A **386** (1997) 348.

[18] B. Andrieu *et al.* [H1 Calorimeter Group Collaboration], Nucl. Instrum. Meth. A **336** (1993) 460.

[19] C. Adloff *et al.* [H1 Collaboration], Eur. Phys. J. C **13** (2000) 609 [hep-ex/9908059].

[20] P. Bruel, "Recherche d'interactions au-delà du Modèle Standard à HERA", Ph.D. Thesis, Université Paris, France, May 1998 (available from http://www-h1.desy.de/psfiles/theses/).

[21] B. Leißner, "Muon Pair Production in Electron-Proton Collisions", Ph.D. Thesis, RWTH Aachen, Germany (in preparation - to be available at http://www-h1.desy.de/psfiles/theses/).

[22] S. D. Ellis and D. E. Soper, Phys. Rev. D **48** (1993) 3160 [hep-ph/9305266].

[23] S. Catani, Y. L. Dokshitzer, M. H. Seymour and B. R. Webber, Nucl. Phys. B **406** (1993) 187.

[24] C. Adloff *et al.* [H1 Collaboration], Nucl. Phys. B **545** (1999) 3 [hep-ex/9901010].

[25] N. Malden, "W production in ep collisions", Ph.D. Thesis, Manchester University, UK, November 2000 (available from http://www-h1.desy.de/psfiles/theses/).

[26] M. Schneider, "Recherche de leptons de grande énergie à HERA", Ph.D. Thesis, Université Louis-Pasteur de Strasbourg, France (in preparation - to be available at http://www-h1.desy.de/psfiles/theses/).

[27] E. E. Boos *et al.*, [hep-ph/9503280].

[28] G. Frising, "Rare Phenomena and W Production in Electron Proton Scattering at HERA", Ph.D. Thesis, RWTH Aachen, Germany (in preparation - to be available at http://www-h1.desy.de/psfiles/theses/).

[29] S. Caron, "Jets in Photoproduction at HERA", Ph.D. Thesis, RWTH Aachen, Germany, September 2002 (available from http://www-h1.desy.de/psfiles/theses/).

[30] C. Adloff *et al.* [H1 Collaboration], Eur. Phys. J. C **25** (2002) 13 [hep-ex/0201006].

Run	Event	Lepton	P_T^l /GeV	P_T^X /GeV	M_T /GeV	$M_{l\nu}$ /GeV	Charge
236176	3849	e	$10.1^{+0.4}_{-0.4}$	$25.4^{+2.8}_{-2.5}$	$26.1^{+1.1}_{-1.1}$		unmeasured
186729	702	μ^+	51^{+11}_{-17}	$66.7^{+4.9}_{-4.9}$	43^{+13}_{-22}		$+$ (4.0σ)
188108	5066	μ^-	$41.0^{+4.3}_{-5.5}$	$26.9^{+2.2}_{-2.3}$	$81.3^{+8.2}_{-11}$	$86.1^{+6.8}_{-8.7}$	$-$ (8.3σ)
192227	6208	μ^-	73^{+9}_{-12}	$60.5^{+5.5}_{-5.4}$	74^{+20}_{-25}		$-$ (7.0σ)
195308	16793	μ^+	60^{+12}_{-19}	$33.3^{+3.6}_{-3.6}$	85^{+25}_{-37}		$+$ (4.2σ)
248207	32134	e^+	$32.0^{+0.8}_{-0.9}$	$42.7^{+3.9}_{-4.1}$	$62.8^{+1.8}_{-1.8}$		$+$ (15σ)
252020	30485	e^+	$25.3^{+1.0}_{-1.0}$	$44.3^{+3.6}_{-3.6}$	$50.6^{+1.9}_{-2.0}$	79^{+12}_{-12}	$+$ (40σ)
266336	4126	μ^+	$19.7^{+0.7}_{-0.8}$	$51.5^{+3.8}_{-4.0}$	$69.2^{+2.4}_{-2.6}$		$+$ (26σ)
268338	70014	e^+	$32.1^{+0.9}_{-0.8}$	$46.6^{+3.3}_{-3.3}$	$87.7^{+2.5}_{-2.4}$		$+$ (5.1σ)
270132	73115	μ	64^{+38}_{-55}	$27.3^{+3.9}_{-3.9}$	140^{+71}_{-83}		$-$ (0.6σ)
275991	29613	e^+	$37.7^{+1.0}_{-1.1}$	$28.4^{+5.7}_{-5.9}$	$74.7^{+2.3}_{-2.4}$		$+$ (37σ)

Table 3: Kinematics and lepton charges of the events at high P_T^X (> 25 GeV). The invariant mass $M_{l\nu}$ is only calculated for those events with an observed scattered electron. The significance of the charge measurement in numbers of standard deviations is given in brackets after the sign. The first event listed was observed in e^-p data. The rest were observed in e^+p data.

Electron	H1 Data	SM expectation	SM Signal	Other SM processes
$P_T^X < 12$ GeV	5	6.40 ± 0.79	4.45 ± 0.70	1.95 ± 0.36
$12 < P_T^X < 25$ GeV	1	1.96 ± 0.27	1.45 ± 0.24	0.51 ± 0.12
$25 < P_T^X < 40$ GeV	1	0.95 ± 0.14	0.82 ± 0.13	0.13 ± 0.04
$P_T^X > 40$ GeV	3	0.54 ± 0.11	0.45 ± 0.11	0.09 ± 0.04

Table 4: Observed and predicted numbers of events in the electron channel for all e^+p data.

Muon	H1 Data	SM expectation	SM Signal	Other SM processes
$12 < P_T^X < 25$ GeV	2	1.11 ± 0.19	0.94 ± 0.18	0.17 ± 0.05
$25 < P_T^X < 40$ GeV	3	0.89 ± 0.14	0.77 ± 0.14	0.12 ± 0.03
$P_T^X > 40$ GeV	3	0.55 ± 0.12	0.51 ± 0.12	0.04 ± 0.01

Table 5: Observed and predicted numbers of events in the muon channel for all e^+p data.

Electron and Muon	H1 Data	SM expectation	SM Signal	Other SM processes
$P_T^X < 12$ GeV	5	6.40 ± 0.79	4.45 ± 0.70	1.95 ± 0.36
$12 < P_T^X < 25$ GeV	3	3.08 ± 0.43	2.40 ± 0.40	0.68 ± 0.14
$25 < P_T^X < 40$ GeV	4	1.83 ± 0.27	1.59 ± 0.26	0.24 ± 0.06
$P_T^X > 40$ GeV	6	1.08 ± 0.22	0.96 ± 0.22	0.12 ± 0.04

Table 6: Observed and predicted numbers of events in the electron and muon channels combined for all e^+p data. Only the electron channel contributes for $P_T^X < 12$ GeV.

	Cross Section / pb			
	Measured	SM NLO	SM LO Diener *et al.*	SM LO Baur *et al.*
$P_T^X < 25$ GeV	$0.146 \pm 0.081 \pm 0.022$	0.194 ± 0.029	0.147 ± 0.044	0.197 ± 0.059
$P_T^X > 25$ GeV	$0.164 \pm 0.054 \pm 0.023$	0.043 ± 0.007	0.041 ± 0.012	0.049 ± 0.015

Table 7: The measured cross section for events with an isolated high energy electron or muon with missing transverse momentum. The cross sections are calculated in the kinematic region: $5^\circ < \theta_l < 140^\circ$; $P_T^l > 10$ GeV; $P_T^{\rm miss} > 12$ GeV and $D_{jet} > 1.0$. Also shown are the signal expectations from the Standard Model where the dominant contribution $ep \to eWX$ is calculated at next to leading order (SM NLO) [5, 7] and at leading order (SM LO) [5] and [6].

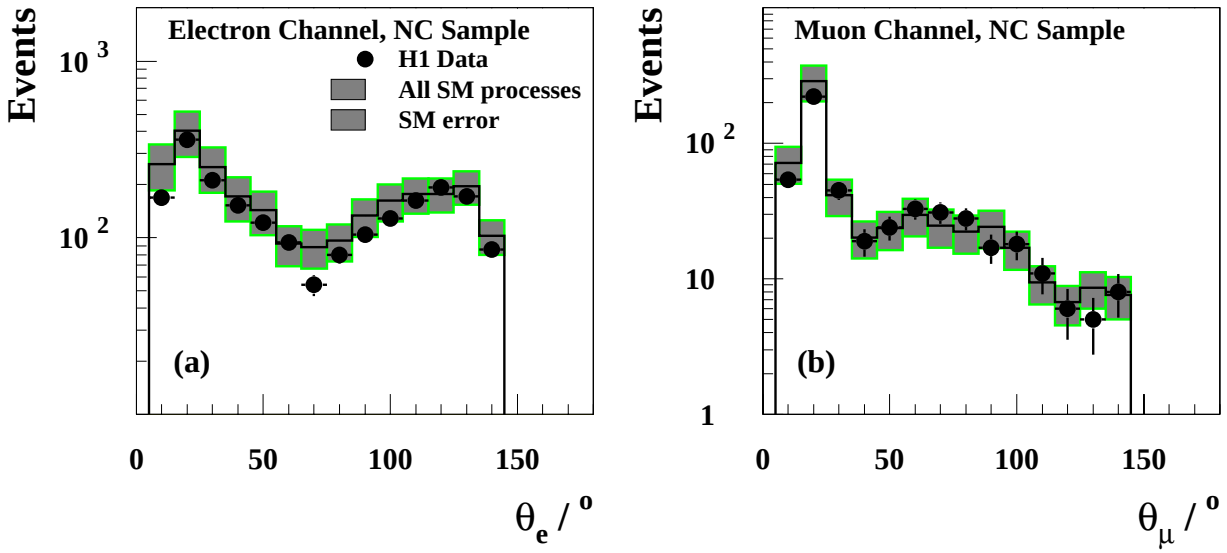

Figure 1: Distributions of lepton polar angle of a second reconstructed electron (a) and a reconstructed muon (b) for NC events. The combined SM expectation is shown as an open histogram. The total error on the SM expectation (see section 7) is given by the shaded band.

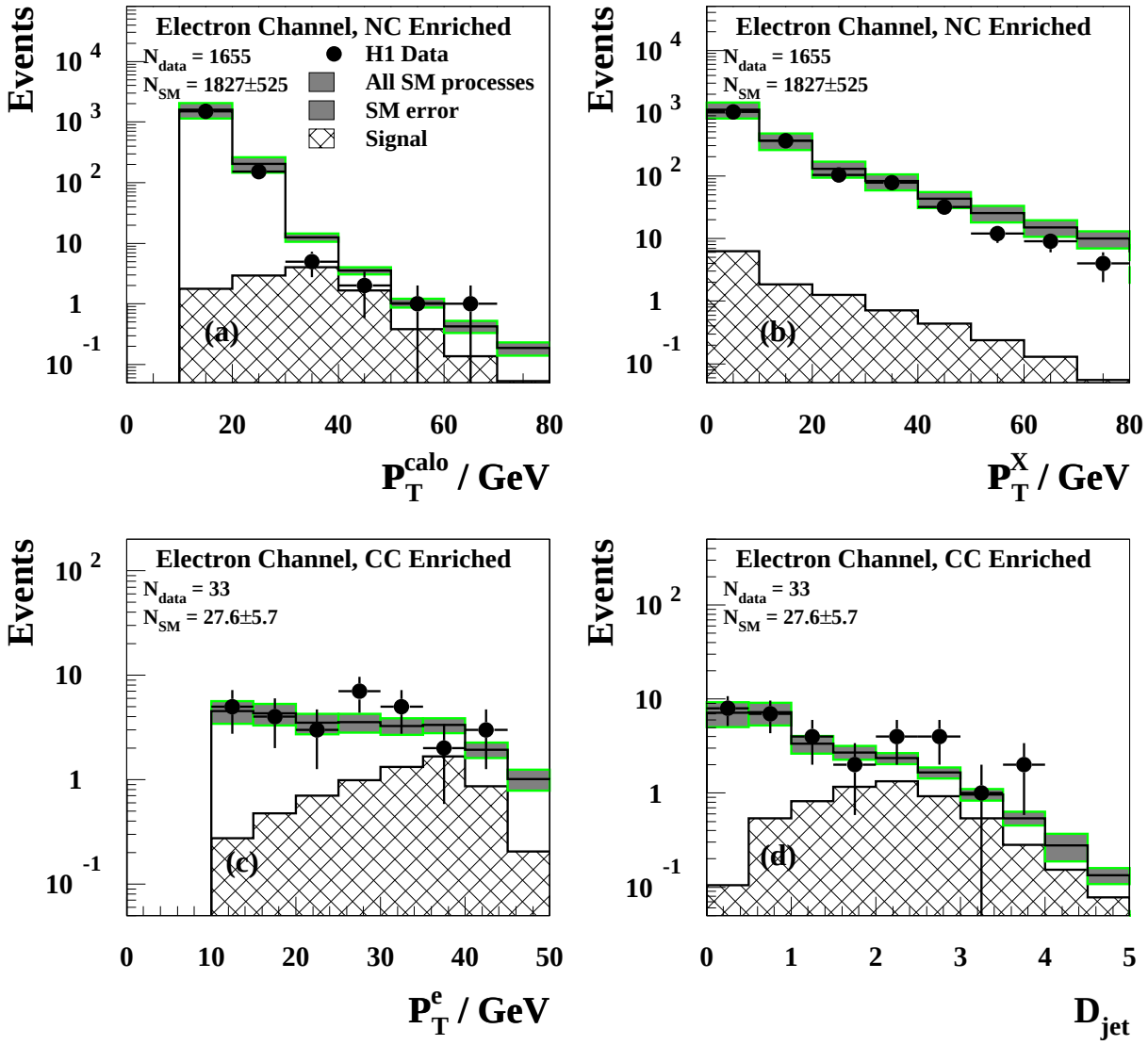

Figure 2: The e^+p data selected in the NC enriched sample (a,b) and in the CC enriched sample (c,d) in the electron channel compared with the combined SM expectation (open histogram). The total error on the SM expectation is given by the shaded band. The "signal" component of the SM expectation is given by the hatched histogram. $\mathrm{N_{data}}$ is the total number of data events observed for each sample. $\mathrm{N_{SM}}$ is the total SM expectation.

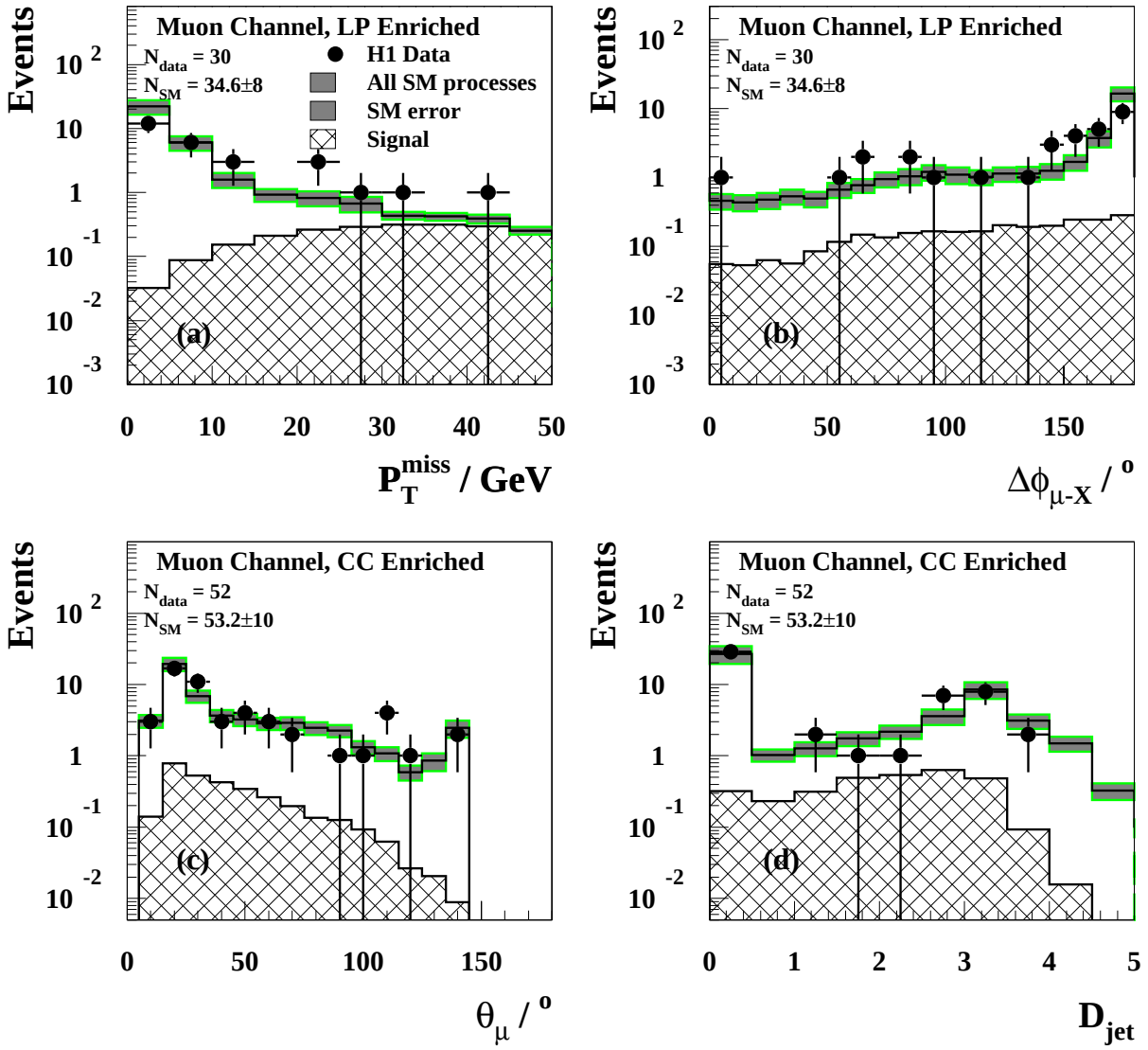

Figure 3: The e^+p data selected in the LP enriched sample (a,b) and in the CC enriched sample (c,d) in the muon channel compared with the combined SM expectation (open histogram). The total error on the SM expectation is given by the shaded band. The "signal" component of the SM expectation is given by the hatched histogram. $\mathrm{N_{data}}$ is the total number of data events observed for each sample. $\mathrm{N_{SM}}$ is the total SM expectation.

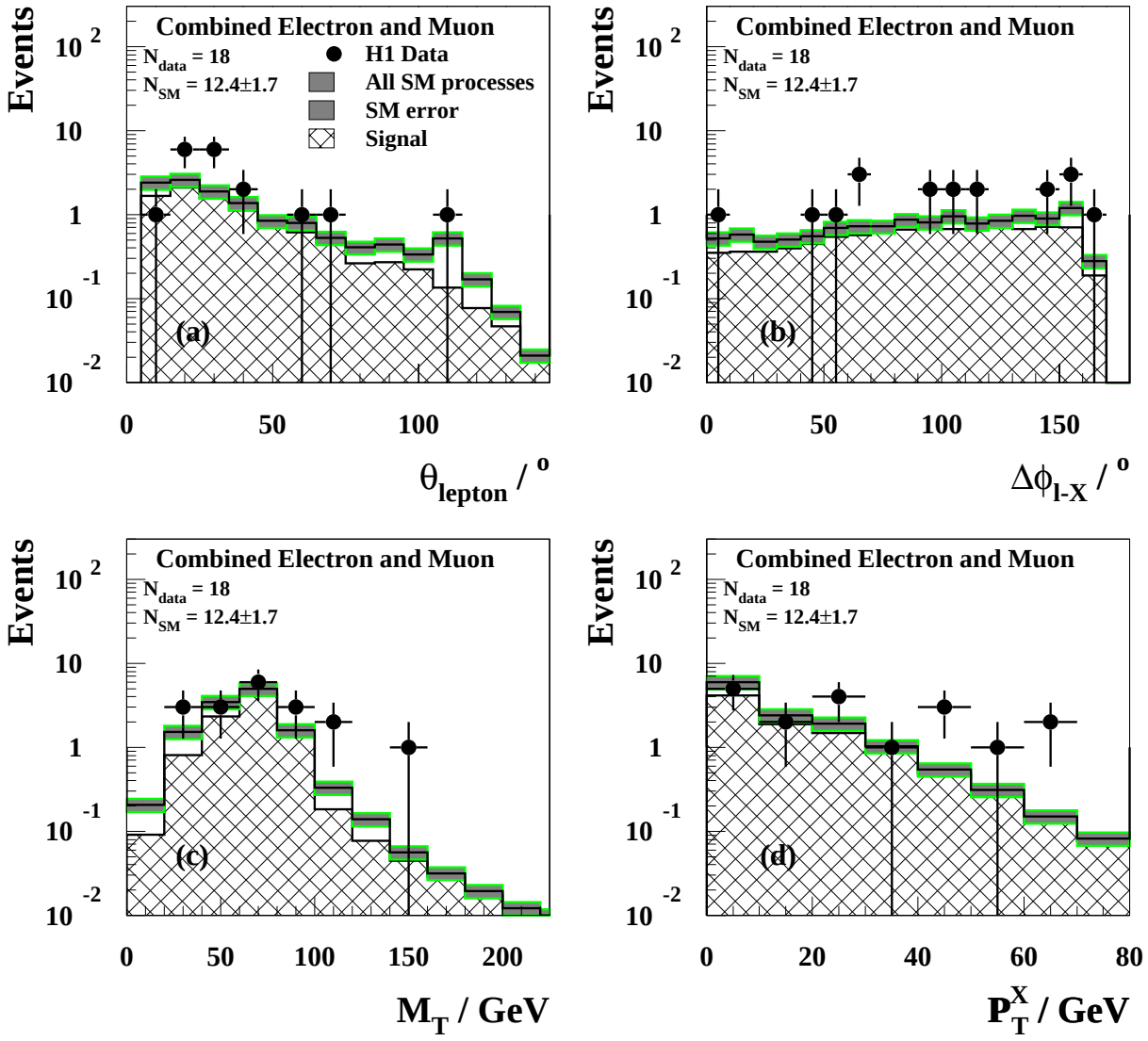

Figure 4: The final e^+p data selection in the electron and muon channels combined compared with the SM expectation (open histogram). The total error on the SM expectation is given by the shaded band. The "signal" component of the SM expectation is given by the hatched histogram. $\mathrm{N_{data}}$ is the total number of data events observed for each sample. $\mathrm{N_{SM}}$ is the total SM expectation.

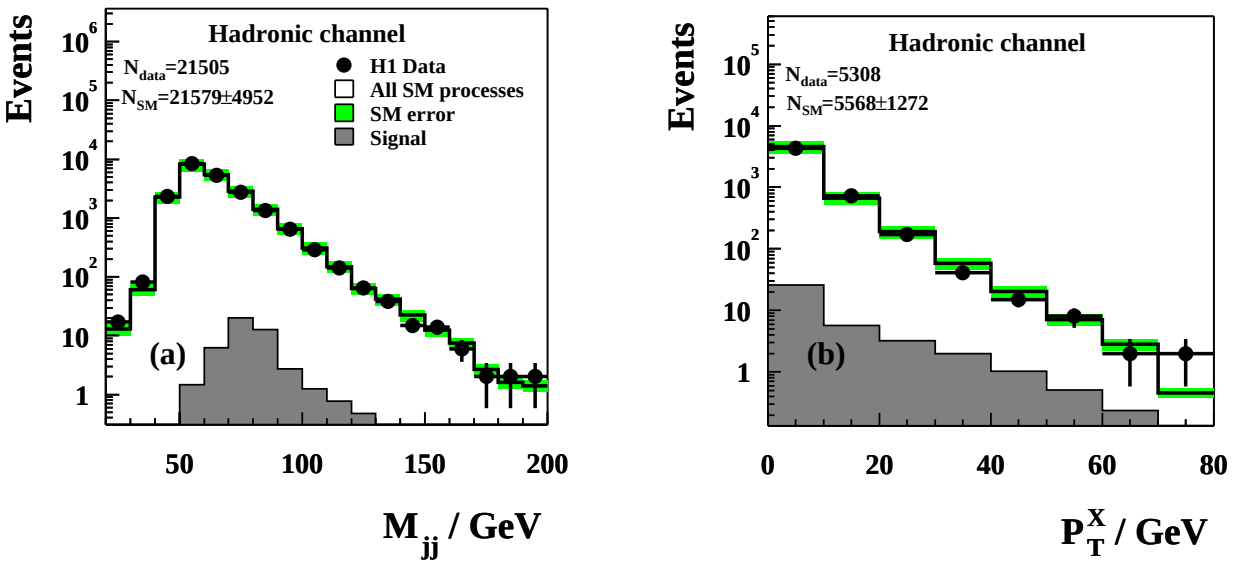

Figure 5: The dijet mass distribution M_{jj} (a) and the P_T^X distribution for $M_{jj} > 70$ GeV (b) compared with the SM expectation (open histogram) in the W hadronic decay channel search. The total error on the SM expectation is given by the shaded band. The W production component of the SM expectation is given by the hatched histogram. $\mathrm{N_{data}}$ is the total number of data events observed for each sample. $\mathrm{N_{SM}}$ is the total SM expectation.